HHS Public Access

Author manuscript

Int J Cancer. Author manuscript; available in PMC 2022 September 17.

LncRNA *PAINT* is associated with aggressive prostate cancer and dysregulation of cancer hallmark genes

Md Faqrul Hasan[1],

Kavya Ganapathy[1],

Jiao Sun[2],

Ayman Khatib[1],

Thomas Andl[1],

Julia N. Soulakova[1],

Domenico Coppola[3,4],

Wei Zhang[2],

Ratna Chakrabarti[1]

[1]Burnett School of Biomedical Sciences, University of Central Florida, Orlando, Florida

[2]Department of Computer Science, University of Central Florida, Orlando, Florida

[3]Moffitt Cancer Center, Tampa, Florida

[4]Florida Digestive Health Specialists, Bradenton, Florida

Abstract

Long noncoding RNAs (lncRNAs) play regulatory role in cellular processes and their aberrant expression may drive cancer progression. Here we report the function of a lncRNA *PAINT* (prostate cancer associated intergenic noncoding transcript) in promoting prostate cancer (PCa) progression. Upregulation of *PAINT* was noted in advanced stage and metastatic PCa. Inhibition of *PAINT* decreased cell proliferation, S-phase progression, increased expression of apoptotic markers, and improved sensitivity to docetaxel and Aurora kinase inhibitor VX-680. Inhibition of *PAINT* decreased cell migration and reduced expression of Slug and Vimentin. Ectopic expression of *PAINT* suppressed E-cadherin, increased S-phase progression and cell migration. *PAINT* expression in PCa cells induced larger colony formation, increased tumor growth and higher expression of mesenchymal markers. Transcriptome analysis followed by qRT-PCR validation

Correspondence: Ratna Chakrabarti, Burnett School of Biomedical Sciences, University of Central Florida, Orlando, FL, USA. ratna.chakrabarti@ucf.edu.

Md Faqrul Hasan and Kavya Ganapathy contributed equally to our study.

CONFLICT OF INTEREST

The authors declare no competing interests.

ETHICS STATEMENT

All human tissues obtained from US Biomax as Tissue Microarrays (TMAs) were collected under HIPPA approved protocols using the highest ethical standards with the donor being informed completely and with their written consent. Xenograft experiments were performed as per relevant guidelines and regulations using an animal protocol approved by the Animal Ethics Committee/Institutional Animal Care and Use Committee of the University of Central Florida.

SUPPORTING INFORMATION

Additional supporting information may be found online in the Supporting Information section at the end of this article.

showed differentially expressed genes involved in epithelial mesenchymal transition (EMT), apoptosis and drug resistance in *PAINT*-expressing cells. Our study establishes an oncogenic function of *PAINT* in PCa.

Keywords

apoptosis; drug resistance; EMT; LncRNA; RNA-Seq

1 | INTRODUCTION

Long noncoding RNAs (lncRNAs) have emerged as key regulatory molecules that play vital roles in gene regulation[1] and are frequently dysregulated in cancers. Due to their heterogeneity, LncRNAs have been integrated in many molecular processes including regulation of genomic integrity, cell fate decisions, differentiation, development, metabolism and cell death.[2,3] Therefore, it is conceivable that lncRNAs also play crucial roles in the initiation and progression of malignancies. Because of their association with tumorigenesis, lncRNAs are becoming novel candidates for therapeutic interventions.

Prostate cancer (PCa) is a commonly diagnosed cancer in American men. Functional vicissitudes of oncogenes and tumor suppressors involving multiple signaling pathways have been implicated in promoting metastatic and drug-resistant PCa.[4] In this regard, a number of aberrantly expressed lncRNAs have significant impacts on the development, metastatic progression and emergence of drug-resistant PCa.[5] For example, lncRNA HOTAIR and SCHLAP1 are commonly upregulated in advanced prostate cancer and promote drug resistance and aggressiveness.[6,7] However, lncRNA MEG3 and LincRNA-p21 are often downregulated in PCa and act as tumor suppressors.[8] Although the functional involvement of a number of lncRNAs has been studied in PCa, a vast majority of dysregulated lncRNAs lack functional characterization and thus may play important roles in PCa progression.

Previously we showed that expression of miR-17–92a microRNA cluster is reduced in aggressive PCa and exhibits a tumor suppressor effect in PCa cells. Restored expression of miR-17–92a cluster inhibited cell proliferation, cell migration, xenograft tumor growth and expression of mesenchymal markers in prostate cancer cells.[9] Transcriptome analysis of miR-17–92a expressing PC-3 cells exhibited dysregulation of several oncogenic and tumor suppressor mRNAs and lncRNAs. Long noncoding RNA *PAINT* was the most downregulated long intergenic noncoding RNA in miR-17–92a expressing PC-3 cells. Here we show functional characterization of the lncRNA *PAINT* (Gene ID: LINC00888, Acc.# NR_038301.1) that promotes PCa progression. We demonstrated that *PAINT* is upregulated in PCa and exhibits a positive correlation with clinical stages of PCa. Our data suggest that *PAINT* promotes PCa phenotypes through upregulation of mesenchymal marker Slug and its target genes by a collective activation of Wnt/β-catenin signaling cascade and genes involved in epithelial-mesenchymal transition (EMT). We also show that inhibition of *PAINT* has a beneficial effect on drug sensitivity of aggressive PCa cells. Our findings provide a novel insight on the role of lncRNA *PAINT* in progression of aggressive PCa.

2 | MATERIALS AND METHODS

2.1 | Patient tissues

PCa tissue microarray (TMA) with 63 cores of de-identified prostate tissues (US Biomax) composed of samples from normal prostate and prostate adenocarcinoma from stages I, II, III and IV were used for analysis of *PAINT* expression. TNM classification and Gleason Scores of samples were included as pathological criteria of the tumors (Supporting Information Table 1).

2.2 | RNA in situ hybridization

Formalin-fixed paraffin embedded (FFPE) TMA slides were used with *PAINT*-specific oligonucleotide probes (NR_038301.1) and positive control probes, which were designed and synthesized by ACD diagnostics and used for automated RNAScope LS assays compatible with Leica Biosystems' BOND RX System. FFPE slides were pretreated and processed for probe hybridization, signal amplification through binding of alkaline phosphatase labeled probes and addition of Fast Red substrate for signal detection using RNAScope 2.5 LS reagents red kit (ACD) and manufacturer's protocol.[10] Individual images were scanned by AperioScope (Leica) and analyzed using QuPath software and expression of *PAINT* were counted as red dots/100 cells.[11] Positive signals were also scored by a pathologist (D.C.) using the Allred scoring system.[12]

2.3 | Cell line maintenance and transfection

PC-3 cells (RRID:CVCL_0035; obtained from ATCC) were cultured in F-12 Kaighn's Modification HAM medium (Sigma Aldrich) containing 10% heat-inactivated Fetal Bovine Serum (FBS) (Atlanta Biologicals) and 1% antibiotic/antimycotic (Life Technologies). C4-2B cells (RRID:CVCL_4784; obtained from ATCC) were maintained in RPMI-1640 media (Sigma Aldrich) containing 10% heat-inactivated FBS and 1% antibiotic/antimycotic. 22Rv1 cells (RRID:CVCL_1045; obtained from ATCC) were maintained in RPMI- 1640 medium containing 10% heat-inactivated FBS and 1% antibiotic/antimycotic. Androgen dependent LNCaP subline LNCaP-104S cells (RRID:CVCL_M126; obtained as a gift from Dr Shutsung Liao from University of Chicago) were maintained in DMEM media (Sigma Aldrich) containing 10% heat-inactivated FBS and 1% antibiotic/antimycotic and 1 ng/mL Dihydrotestosterone (DHT) (Life Technologies). MDA-PCa-2b cells (RRID:CVCL_4748; obtained from ATCC) were maintained in 10% F-12 K medium containing 10% nonheat inactivated FBS, 1% antibiotic/antimycotic, 25 ng/mL cholera toxin, 10 ng/mL mouse EGF, 0.005 mM phosphoethanolamine, 100 pg/mL hydrocortisone, 45 nM sodium selenite, 0.005 mg/mL human. Recombinant insulins. Both LNCaP C4-2B and LNCaP 104-S are derivatives of LNCaP (RRID: CVCL_0395). All cell lines have been authenticated using short tandem repeat profiling within the last 3 years and tested for mycoplasma contamination by DAPI staining. All experiments were performed with mycoplasma-free cells.

PC-3 cells were transfected with *PAINT* siRNA smart pool PC-3-*PAINT*^{si} and nontargeting siRNA pool PC-3^{C} (negative control) (Dharmacon) using RNAiMAX (Invitrogen) for knockdown studies. Cells were harvested 48 or 72 hours after transfection for subsequent

experiments. For overexpression studies, *PAINT* overexpressing C4-2B subline (C4-2B-*PAINT*$^{++}$and control C4-2B (C4-2B^{C}) subline were generated by transfecting C4-2B cells with either pcDNA3.1 + *PAINT* or pcDNA3.1+control using Lipofectamine 3000 (Invitrogen). Colonies were selected by treating transfected C4-2B cells with 1 mg/mL of G-418 (KSE Scientific) for 3 weeks and cloned for generating stable sublines. *PAINT* overexpression was determined using qRT-PCR for each subline and used for relevant experiments. Additionally, an inducible stable line was constructed by transfecting C4-2B cells with pLVX-TetOne-*PAINT* using Lipofectamine 3000 transfection reagent (ThermoFisher Scientific) and selected for stable sublines using puromycin. Doxycycline-induced C4-2B-*PAINT* cells (C4-2B-*PAINT*^{I}) were used in comparison to the uninduced stable line (C4-2B-*PAINT*^{UI}) serving as controls. For in vivo experiment, both constitutive stable lines (C4-2B-*PAINT*$^{++}$ and control C4-2B C4-2B^{C}) and the inducible stable line (C4-2B-*PAINT*^{I}) were used. *PAINT* overexpression was determined using qRT-PCR for each constitutive and inducible (with or without induction) subline and used for relevant experiments.

2.4 | Quantitative real-time PCR

Total RNA was extracted from different PCa cell lines using Direct-zol quick miniprep plus RNA extraction kit (Zymo Research). cDNA was synthesized from extracted RNA using RT^{2} First Strand Kit (Qiagen) or High-Capacity cDNA Reverse Transcription Kit (Applied Biosystems) as suppliers' recommendation. Expression of *PAINT* was determined using *PAINT*-specific primer pairs (RT^{2} qPCR Primer Assays - Qiagen) and internal control EIF3D and RPL13A specific primers (RT^{2} qPCR Primer Assays-Qiagen) and RT^{2} SYBR Green qPCR master mix using the recommended protocol. Quantitative RT-PCR was performed in a QuantStudio 7 thermal cycler (Applied Biosystems) and was quantified based on SYBR green fluorescence and normalized based on the passive reference dye, ROX. Acquired data was analyzed based on $2^{-\Delta\Delta CT}$ Livak-method and our published study[12] to identify expression of PAINT in relevant experiments.

2.5 | Western blotting

Total protein lysates were prepared from PC-3-*PAINT*^{si}, PC-3^{C} and C4-2B-*PAINT*$^{++}$ and C4-2B^{C} sublines using RIPA buffer supplemented with phosphatase and protease inhibitors (Fisher Scientific) and used for immuno-blotting using anti-Slug, anti-Vimentin, anti-E-cadherin, anti- PARP, anti-cleaved-Caspase 3, anti-Beta-Catenin, anti-phospho-AKT, pan-Akt, alpha-tubulin and anti-GAPDH (Cell Signaling Technology), and anti-PCNA (Santa Cruz). Alpha-Tubulin or GAPDH were used as internal controls. Blots were imaged using ECL chemiluminescence substrates and imaged with ChemiDoc MP Imaging System (Bio-Rad). Comparative expression was performed based on densitometry analysis using Image J software.

2.6 | Drug sensitivity assay

For drug sensitivity assay, transfected PC-3 cells were seeded in 96 well plates and transfected with siRNAs. At 24 hours after transfection, cells were treated with DTX at 5 nM and 25 nM or VX-680 at 1 μM or DMSO as the control and continued incubation

for additional 48 hours. MTS assays were performed to quantify viable cells at different experimental conditions.

2.7 | In vivo xenograft animal study

Xenograft experiments were performed using 6–8 weeks old NSG (NOD.Cg-PrkdcscidIl2rgtm1Wjl/SzJ [005557]) mice (Jackson Laboratory) maintained under pathogen-free conditions. Xenograft experiments were performed as per guidelines established and using an animal protocol approved by the Animal Ethics Committee/ Institutional Animal Care and Use Committee of the University of Central Florida. NSG mice were injected with C4-2B-*PAINT*$^{++}$, control C4-2B^{C} cells or with inducible C4-2B-*PAINT*^{I} cells. For all mice, 6×10^6 cells /mouse mixed with 0.1% matrigel in a 100 μL total volume were injected subcutaneously into the flank. For the inducible cells, once tumor volume reached 300 mm^3, animals were randomly separated into uninduced or induced group receiving Dox-feed (625 mg Doxycyline/kg, Envigo Teklad Diets) to monitor tumor growth with a caliper. For constitutive C4-2B-*PAINT*$^{++}$ and control C4-2B^{C} cells, tumor growth was monitored since the week of development of visible tumors. Tumor volume was calculated as 0.52 × length × height × width as the tumors grew. Tumors were harvested after the specified time and tumors were used for RNA extraction followed by qRT-PCR analysis of *PAINT* expression.

2.8 | Preparation of RNA samples for next gen RNA-sequencing

Total RNA was depleted of rRNAs using Arraystar rRNA removal kit and used for library preparation using Illumina kit for the RNA-seq library preparation. This includes RNA fragmentation, random hexamer priming for the first stand and dUTP based second strand synthesis followed by A tailing and adapter ligation. Next PCR amplification was performed for generating cDNAs for library preparation. The quality of the RNA library was checked for integrity of fragments between 400–600 bases Agilent 2100 Bioanalyzer and quantified using qRT-PCR through absolute quantification. DNA fragments were denatured using 0.1 M NaOH and sequencing was performed in Illumina NovaSeq 6000 after fragments were amplified using NovaSeq 6000 S4 Reagent Kit for 150 cycles. RNA-Seq library preparation, sequencing and data analysis were performed by Arraystar Inc. The Raw data file in FASTQ format was subjected to quality control plot using FastQC software to obtain a quality score. All samples had a Q ≥ 30 score of ≥93. Next, the fragments were adapter trimmed and filtered ≤20 bp reads using cutadapt software, and trimmed fragments aligned to reference genome (including mRNA, pre-mRNA, poly-A tailed lncRNA and pri-miRNA) with HiSAT2[13] software. More than 92% of the reads of the trimmed pairs were aligned with the reference genome.

2.9 | RNA sequencing and data analysis

Whole genome transcription profiling except ribosomal RNAs (rRNAs) and transfer RNAs (tRNAs) was performed using C4-2B-*PAINT*$^{++}$ or C4-2B^{C} cells. Quantification of FPKM values and differentially expressed gene and transcript analyses were performed using R package Ballgown. Fold change (cutoff 1.5), *P*-value (≤.05) and FPKM (≥ 0.5 mean in one group) were used for filtering differentially expressed genes and transcripts. GO enrichment analysis was used to associate the differentially expressed genes to specific GO

terms. Pathway analysis using KEGG database was done for determining the enrichment of specific pathways by the differentially expressed genes. The *P*-values calculated by Fisher's exact test was used to estimate the statistical significance of the enrichment of GO terms and pathways between the two groups. All other analysis and statistical computing were performed using R, Python and Shell environment by Arraystar Inc. The sequencing coverage and quality statistics for each sample are summarized in Supporting Information Table 8.

2.10 | Statistical analysis

For TMA analysis, the key measures of interest (dependent variables) were the average number of red spots per 100 cells in a section computed over three sections from the same tumor tissue; the average was treated as a continuous variable. Supporting Information Table 4 presents the summary statistics for the three numbers (termed targets) and the average number. Additional measures (independent variables) for cancer tissues included cancer stage (I/II, III, IV), grade, Gleason score indicator (GSI) that differentiated between "low" (6 or less) and "high" (7 or greater), and metastasis indicator that differentiated between tissues with (TNM contained N1, N2, M1, M1b, or M1c) and without metastases (TNM contained none of N1, N2, M1, M1b, and M1c). We also used a multinomial regression model, Kaplan-Meier estimation, one-way ANOVA and two-sample *t*-tests. The significance levels were fixed at the 5% level (*P*-value ≤ .05) or for some results at 10% level (*P*-value ≤ .1). Multiple comparisons were performed using Bonferroni adjustments. Analyses were performed using SAS9.4 software.[14] Data were represented as mean ± SD.

Methodologies of all phenotypic experiments such as cell proliferation, flow cytometry and Annexin V apoptosis assays, migration and colony formation assays and immunofluorescence assays are provided in the Supporting Information methods sections.

3 | RESULTS

3.1 | *PAINT* is upregulated in aggressive PCa

To explore the expression of *PAINT* in PCa, we performed *PAINT* RNA-in-situ hybridization (RNA-ISH) using PCa TMA comprised of normal prostate tissues and prostate adenocarcinomas with pathological criteria of stages I/II, III and IV (Supporting Information Table 1). We noted overexpression of *PAINT* in prostate tumors compared to the normal prostate tissues specifically, in late stage PCa (stage III and stage IV) compared to early stage PCa (Figure 1A,B and Supporting Information Figure S7). Group sample sizes for the statistical analysis and the summary statistics for the primary measures for cancer and normal tissues are shown in Supporting Information (Supporting Information Tables 2 and 3).

The summary statistics showed that the model for *PAINT* expression was significant (F = 342.6, df = 7, P-value < .001, R^2 = 0.47) and indicated significance of stage (P-value < .001) and metastasis (P-value < .001) (Supporting Information Table 4). Analysis showed significant differences between stages I/II and IV (adjusted P-value < .003) and stages III and IV (adjusted P-value = .039). We note that grade was significant at 10% level (P-value

= .057). Analysis of the prediction of PCa stages incorporated a multinomial regression model (Likelihood ratio X^2 = 16.5, df = 8, *P*-value = .036, R^2 = 0.27) for the logit of probability of stage IV vs stage I/II and probability of stage III vs stage I/II. Our results showed that *PAINT* expression was a significant predictor overall (*P*-value = .010) and of the odds of cancer stage IV relative to stage I/II (OR = 1.30, 95% CI = 1.10:1.54, *P*-value = .03) (Figure 1C and Supporting Information Table 5). Analysis of TCGA PRAD[15] dataset further revealed higher expression of *PAINT* in late stage PCa tissues and was correlated to poor survival (Figure 1D, Supporting Information Figure S1A). Analysis of *PAINT* expression in PCa cell lines showed its highest expression in metastatic PC-3 cells compared to other PCa cell lines (Figure 1E). Collectively, these observations demonstrate that *PAINT* is upregulated in PCa tissues exhibiting a direct correlation with tumor stages and metastatic PCa.

3.2 | *PAINT* regulates cell phenotype and drug sensitivity in PCa cells

The functional role of *PAINT* in PCa was determined using knockdown and overexpression approaches. siRNA-based inhibition of *PAINT* in PC-3 cells (PC-3-*PAINT*^{si}) and ectopic expression of *PAINT* in C4-2B cells (C4-2B-*PAINT*$^{++}$) were used for subsequent studies. Knockdown and overexpression of *PAINT* in PC-3 and C4-2B respectively, were confirmed by qRT-PCR analysis (Supporting Information Figure 1C,D). PC-3-*PAINT*^{si} cells exhibited an altered cell morphology from its spindle shape to a more epithelial cuboidal shape (Supporting Information Figure S1B), reduced cell proliferation (26%) (Figure 2A) and S-phase cells (Figure 2C; Supporting Information Figure S2A) compared to the control PC-3 (PC-3^{C}) cells. Instead, C4-2B-*PAINT*$^{++}$ cells exhibited increased cell proliferation (53%) (Figure 2B), higher Ki67 proliferation index[16] (Supporting Information Figure S1E) and an enrichment in S-phase cell population (Figure 2D and Supporting Information Figure S2B) compared to control C4-2B (C4-2B^{C}) cells. Expression of S-phase marker PCNA[17] showed increased expression (40%) in C4-2B-*PAINT*$^{++}$ cells (Figure 2F and Supporting Information Figure S2D) and reduced expression (18%) in PC-3-*PAINT*^{si} cells (Figure 2E and Supporting Information Figure S2C) suggesting that *PAINT* expression influences cell cycle progression and cell proliferation.

Next, analysis of cell survival showed increased expression of cleaved-Caspase 3 (1.5-fold) and cleaved PARP (2.5-fold) in PC-3-*PAINT*^{si} compared to PC-3^{C} cells (Figure 2G,H and Supporting Information Figure S2E). This led us to examine the effect of *PAINT* inhibition on drug sensitivity of PC-3 cells to docetaxel (DTX) and VX680 (Aurora kinase inhibitor).[18,19] DTX and VX680 treatment showed an additive effect with *PAINT* inhibition, on reduced cell viability at ~20% and 10% levels, respectively compared to control (Figure 2I,J). Annexin-V apoptosis assays showed a significant increase in the percentage of apoptotic cells upon treatment with DTX and VX-680 in PC-3-*PAINT*^{si} cells compared to PC-3^{C} cells (Figure 2K and Supporting Information Figure S2F). These results suggest that *PAINT* supports cell survival by evading apoptosis and decreasing the efficacy of therapeutic agents.

3.3 | *PAINT* promotes colony formation of PCa cell and tumor growth in xenograft models

Next, we examined the effect of *PAINT* overexpression on anchorage independent colony formation and in vivo effect of *PAINT* expression on tumorigenicity in animal models. We noted a higher percentage (52%) of large colonies (>70 μm) in C4-2B-*PAINT*$^{++}$ cells compared to C4-2B^{C} cells (19%) (Figure 3A,B). We also noted a significantly increased rate of tumor growth for the mice injected with C4-2B-*PAINT*$^{++}$ compared to the control C4-2B^{C} cells (Figure 3C and Supporting Information Figure S3C). Mice injected with the inducible *PAINT*-expressing C4-2B cells (C4-2B-*PAINT*) showed a significantly shorter survival time compared to the uninduced controls (C4-2B-Control) (Figure 3D). qRT-PCR analysis of tumor tissues from mice injected with C4-2B-*PAINT*$^{++}$ cells exhibited significantly higher expression of *PAINT* compared to the control (Figure 3E). This observation aligns with our in vitro studies and confirms a tumor promoting role of *PAINT*.

3.4 | *PAINT* promotes migration and EMT in PCa cells

Next, we examined the involvement of *PAINT* in cell migration and EMT that are important hallmarks of cancer. Scratch assays showed a 34% increased rate of migration of C4-2B-*PAINT*$^{++}$ cells compared to C4-2B^{C} cells (Figure 4B and Supporting Information Figure S3B), whereas inhibition of *PAINT* expression showed an opposite effect (Figure 4A and Supporting Information Figure S3A). Since EMT is frequently associated with metastatic and aggressive behavior, we focused on the relationship between *PAINT* and the key mesenchymal marker Slug.[20,21] Inhibition of *PAINT* expression in PC-3-*PAINT*^{si} reduced Slug by 57% compared to PC-3^{C} cells. Regarding Slug-target genes, *PAINT* inhibition reduced Vimentin expression (87%), a Slug-induced gene,[21] and increased E-cadherin expression (40%), a Slug-repressed gene[22] (Figure 4C–F). Overexpression of *PAINT* in C4-2B-*PAINT*$^{++}$ reversed these effects showing an increase (96%) in Slug expression and a decrease (30%) in E-cadherin expression compared to C4-2B^{C} cells (Figure 4G–I).

As induction of EMT is often associated with activation of different signaling pathways, we monitored β-catenin expression which promotes EMT through Slug expression.[23] A significant downregulation of β-catenin was noted in PC-3-*PAINT*^{si} cells (Figure 4J,K). We also determined Akt activation, which can induce EMT and metastasis through Slug regulation,[24] upon *PAINT* overexpression. Our results showed an increased expression of phospho-AKT while Akt levels remained unchanged compared to C4-2B^{C} cells (Figure 4L,M). These observations indicate a role of *PAINT* in activating multiple signaling pathways that promote PCa progression and EMT.

3.5 | Transcriptome analysis revealed altered gene expression in PCa cells expressing *PAINT*

To understand the cellular reprograming behind the potential oncogenic role of *PAINT* in PCa progression, we performed RNA-seq analysis of C4-2B-*PAINT*$^{++}$ (group E) and C4-2B^{C} cells (group C). The short reads were aligned to the human GRCh37 reference genome by HiSAT2.[13] Sequencing statistics of each sample is presented in Supporting Information Table 8.

The abundance of genes and transcripts represented by FPKM values in the two group of samples were estimated by StringTie.[25] Pearson correlation analysis showed a strong correlation (>0.997) between *PAINT* overexpressing cells and control cells (Figure S4A). Using R package ballgown,[26] a total of 76 upregulated genes and 61 downregulated genes with fold-change >1.5 and *P*-value < .05 were identified in *PAINT*-expressing cells compared to control cells. A volcano plot based on $\log_2$ of fold change vs $-\log_{10}$ of *P*-values of the genes showed a large magnitude of statistically significant changes between C4-2B *PAINT*-expressing cells compared to control cells (Figure S6A, and Supporting Information Tables 6 and 7). Chromosomal mapping of dysregulated genes indicates that chromosomes 1, 11 and 19 contain the majority of the upregulated genes and chromosomes 1, 2 and 6 contain the majority of the downregulated genes (Figure S6B). Unsupervised hierarchical clustering grouped the majority of differentially expressed genes based on their FPKM values (Figure 5A) showing distinct sets of genes that are upregulated or downregulated in *PAINT* expressing cells. Principal component analysis (PCA) shows distinct clustering of samples with genes that have *P*-value < .05 on FPKM abundance estimation (Figure 5B). In addition, 9086 novel genes were identified using CPAT (Coding Potential Accessing Tool),[27] which showed distinct clusters of potentially protein coding and noncoding genes (Supporting Information Figure S4B). Altogether, transcriptome analysis revealed a set of genes that were altered upon overexpression of *PAINT*.

3.6 | Identification of functionally related groups and enrichment of pathways of dysregulated genes in *PAINT*-expressing cells

Gene ontology (GO) analysis of top dysregulated genes was performed based on specific gene attributes such as biological process (BP), molecular function (MF) and cellular component (CC). Circular plots show the GO enrichment of the top downregulated genes (Figure 6A and Supporting Information Figure S4C and S4D) and upregulated genes (Figure 6C and Supporting Information Figure S4E and S4F) in C4-2B-*PAINT*$^{++}$ cells based on BP, CC and MF respectively. Furthermore, significantly downregulated (Figure 6B) and upregulated genes (Figure 6D) were grouped based on the top 10 enriched GO terms within BP, CC and MF. Furthermore, KEGG Pathway analysis of upregulated and downregulated genes revealed multiple pathways that showed >1.5 enrichment score (−log10 [p_value]) (Supporting Information Figure S5A–E and Supporting Information Figure S5F–I). Taken together, GO and KEGG pathway analysis establish that *PAINT* expression is associated with regulation of gene expression involved in several BPs, functions and pathways which possibly contribute to prostate cancer progression.

3.7 | *PAINT*-expressing C4-2B cells reveal altered expression of gene targets involved in the EMT and apoptosis network that may regulate *PAINT*-induced PCa progression

Further analysis of the RNA-Seq data revealed a set of significantly dysregulated genes in *PAINT* expressing cells that were involved in EMT, apoptosis and drug sensitivity processes, similar to our observations from in vitro characterization studies (Figure 7A,B). The clinical significance of these genes in PCa progression was examined next using TCGA PRAD dataset (n = 623). Our analysis identified two downregulated genes, TMEFF2[28] (Figure 7H) and SLC22A3[29] (Figure 7I) that showed decreased expression with stage-specific progression of PCa and five upregulated genes, TMPRSS4[30] (Figure 7C), SYT4[31] (Figure

7D), SESN3[32] (Figure 7E), CRISP3[33] (Figure 7F) and NANOS3[34] (Figure 7G) that showed increased expression associated with stage specific progression of PCa. qRT-PCR analysis validated overexpression of selected five upregulated genes (Figure 7J) and reduced expression of two selected downregulated genes (Figure 7K). Altogether, our findings suggest that *PAINT* regulates a group of genes involved in cell growth, drug resistance and EMT, all of which come together to drive PCa progression to more aggressive stages.

4 | DISCUSSION

Emerging studies established the role of aberrantly expressed lncRNAs in several cancers including PCa.[35] Here, we focused on describing the function of a novel lncRNA and its role in PCa progression through modulation of specific gene networks. Our previous studies identified a tumor suppressor microRNA cluster, miR-17–92a, that is downregulated in PCa.[9] RNA-seq analysis of PC-3 cells with restored miR-17–92a cluster miRNAs showed altered expression of several intergenic lncRNAs having more than a 2-fold change ($\log_2$) in expression, out of which *PAINT* was the most downregulated lncRNA. Expression of this lncRNA is upregulated in melanoma[36] but no information on the involvement of *PAINT* in PCa progression is available. Hence, we chose *PAINT* for further study on its role in PCa progression. To our knowledge, this is the first study that shows an oncogenic function of *PAINT* in PCa.

Our study revealed *PAINT* overexpression in prostate tumors and in metastatic PCa. TCGA data analysis further showed a positive correlation of *PAINT* with advanced stages of PCa with poor patient survival. Similarly, *PAINT* was upregulated in metastatic and drug-resistant PCa cell line compared to the less aggressive PCa cell lines. Collectively, *PAINT* upregulation in PCa, especially in the later stages, suggested the possibility of *PAINT* being a driver oncogene promoting progression of metastatic PCa.

The oncogenic function of *PAINT* was supported by the results showing *PAINT*-induced increased proliferation, migration, larger colony formation and EMT marker expression while most of these effects were blunted upon *PAINT*-siRNA expression. We used a stable C4-2B subline expressing 6-fold higher amounts of *PAINT* compared to the vector only control C4-2B cells. The expression is within the physiological level of expression as the endogenous level of *PAINT* in PC-3 cells is 11-told higher than that of the parental C4-2B cells. Our xenograft studies showed increased tumor growth and reduced survival of mice injected with C4-2B-*PAINT* cells compared to control cells, which further confirmed the oncogenic role of *PAINT*. *PAINT* overexpression also facilitates cell survival as inhibition of *PAINT* induced apoptosis through activation of proteins involved in the apoptotic pathways[37] and as a result, significantly improved the sensitivity of drug-resistant PC-3 cells to chemotherapeutic agents. These results highlight the importance of *PAINT* as a potential therapeutic target for PCa management.

Another hallmark of aggressive cancer is increased cell migration which contributes to the metastatic potential of cancer cells.[38] EMT enhances invasive migratory properties of cancer cells and plays an important role in cancer metastasis[39] while biomarkers of EMT, including Slug and E-cadherin, are involved in regulation of prostate cancer cell migration.[39,40] Our

results showed *PAINT*'s involvement in cell migration and a positive correlation of *PAINT* with Slug expression. Slug, one of the major transcription factors involved in EMT,[40] promotes cell migration and invasion through modulation of different signaling pathways.[41] As we noted, upregulation of Slug was associated with an increased expression of Vimentin, a Slug effector and a decreased expression of E-cadherin that is negatively regulated by Slug.[42,43] Our results showing reduced β-Catenin expression in PC-3-*PAINT*^{si} cells and increased phospho-Akt in C4-2B-*PAINT*$^{++}$ cells further suggest the involvement of Wnt signaling[44] and PI3K/Akt[45] signaling circuitries that affect Slug expression. Beta-Catenin, a key Wnt signaling pathway protein, regulates Slug expression and EMT transition via Vimentin and E-cadherin,[40] while phospho-Akt regulates Slug expression via PI3K/Akt pathway.[24] Both Wnt signaling[44] and PI3K/Akt[45] pathways are constitutively activated in PCa promoting cancer progression, metastasis and drug resistance. The cross-talk between signaling pathways further established the role of *PAINT* in the regulation of EMT related genes and cell migration and activation of multiple signaling cascades that contribute to PCa metastasis. This phenomenon has been further evaluated during unbiased RNA-seq data analysis.

Transcriptome profiling further complements the phenotypic characterization data of *PAINT* and provided a comprehensive understanding of genes involved in promoting PCa progression upon *PAINT* dysregulation. GO enrichment and KEGG pathway analysis revealed altered expression of genes and pathways indicating that *PAINT* may promote an oncogenic environment by simultaneously regulating various processes in PCa. Consistent with our observations from the *PAINT* expression associated phenotypic changes, transcriptome profiling identified a specific set of dysregulated genes involved in EMT, apoptosis and drug resistance. TCGA PRAD dataset analysis corroborated with our RNA-Seq data showing overexpression of TMPRSS4, SYT4, SESN3, CRISP3 and NANOS3 and reduced expression of TMEFF2 and SLC22A3 in PCa, which were further validated by qRT-PCR.

TMPRSS4 is overexpressed in PCa and other cancers,[46] and is involved in EMT induction, specifically through modulation of Slug expression[30] and drug resistance.[47] SYT4 is a neuroendocrine marker that is overexpressed during transition from localized to metastatic PCa[31] and in drug-resistant LNCaP cells.[31] SESN3 (Sestrin 3) is implicated in promoting EMT[48] and inhibiting apoptosis in PCa.[49] Inhibition of SESN3 increased sensitivity of drug-resistant PCa to cabazitaxel.[32] CRISP3 and NANOS3 are highly upregulated in multiple cancers and promote EMT, migration and invasion.[33,34] TMEFF2 functions as a strong tumor suppressor by suppressing migration and invasion in PCa cells,[50] and overexpression of TMEFF2 induced apoptosis in panceraric cancer cells.[51] SLC22A3 is also downregulated in aggressive PCa[29] and functions as a direct inhibitor of EMT in esophageal cancer.[52] These findings provide convincing evidence that *PAINT* plays an oncogenic role through modulation of different signaling molecules specifically involved in EMT, apoptosis and drug resistance, which collectively play an integrated role in PCa progression to a more aggressive and metastatic stage.

In summary, our findings establish *PAINT* as an oncogene in PCa and indicate the clinical significance of *PAINT* as a diagnostic marker and a possible therapeutic target for aggressive

PCa. However, in-depth mechanism of *PAINT* mediated regulation of these cellular events, which promote PCa progression and metastasis remains unclear. Our future studies will focus on the mechanistic role of *PAINT* in functional regulation of different target genes and their involvement in the progression of aggressive disease.

Supplementary Material

Refer to Web version on PubMed Central for supplementary material.

ACKNOWLEDGMENTS

We thank Dr Shaojie Zhang, Department of Computer Science, University of Central Florida, for his valuable comments and help in experimental design. Our study is supported by a grant from National Cancer Institute, National Institutes of Health (R21CA226611) to Ratna Chakrabarti.

Funding information

National Institutes of Health, Grant/Award Number: R21CA226611

DATA AVAILABILITY STATEMENT

The RNA-Seq data generated in this study is available in GEO under accession # GSE158953. All other data that support the findings of this study are available from the corresponding author (ratna. chakrabarti@ucf.edu) upon reasonable request.

Abbreviations:

BP	biological process
C4-2B^{C}	control C4-2B cells without ectopic expression of *PAIN*
C4-2B-*PAINT*$^{++}$	C4-2B cells ectopic expressing *PAINT*
CC	cellular component
CPAT	coding potential accessing tool
DTX	docetaxel
EMT	epithelial-mesenchymal transition
FFPE	formalin-fixed paraffin embedded
GO	gene ontology
GSI	Gleason score indicator
LncRNAs	long noncoding RNAs
MF	molecular function
PAINT	prostate cancer associated intergenic noncoding transcript
PCa	prostate cancer

PC-3-*PAINT*^{si}	siRNA-based inhibition of *PAINT* in PC-3 cells
PC-3^{C}	nontargeting siRNA pool transfected in PC-3
RNA-ISH	RNA in situ hybridization
ROC	receiving operator characteristics
rRNAs	ribosomal RNAs
TCGA PRAD	The Cancer Genome Atlas Prostate Adenocarcinoma Dataset
TMA	tissue microarray
tRNAs	transfer RNAs
VX680	Aurora kinase inhibitor

REFERENCES

1. Ransohoff JD, Wei Y, Khavari PA. The functions and unique features of long intergenic non-coding RNA. Nat Rev Mol Cell Biol. 2018;19(3): 143–157. [PubMed: 29138516]
2. Fatica A, Bozzoni I. Long non-coding RNAs: new players in cell differentiation and development. Nat Rev Genet. 2014;15(1):7–21. [PubMed: 24296535]
3. Sun Q, Hao Q, Prasanth KV. Nuclear long noncoding RNAs: key regulators of gene expression. Trends Genet. 2018;34(2):142–157. [PubMed: 29249332]
4. Semenas J, Allegrucci C, Boorjian SA, Mongan NP, Persson JL. Overcoming drug resistance and treating advanced prostate cancer. Curr Drug Targets. 2012;13(10):1308–1323. [PubMed: 22746994]
5. Evans JR, Feng FY, Chinnaiyan AM. The bright side of dark matter: lncRNAs in cancer. J Clin Invest. 2016;126(8):2775–2782. [PubMed: 27479746]
6. Zhang A, Zhao JC, Kim J, et al. LncRNA HOTAIR enhances the androgen-receptor-mediated transcriptional program and drives castration-resistant prostate cancer. Cell Rep. 2015;13(1): 209–221. [PubMed: 26411689]
7. Prensner JR, Iyer MK, Sahu A, et al. The long noncoding RNA SChLAP1 promotes aggressive prostate cancer and antagonizes the SWI/SNF complex. Nat Genet. 2013;45(11):1392–1398. [PubMed: 24076601]
8. Luo G, Wang M, Wu X, et al. Long non-coding RNA MEG3 inhibits cell proliferation and induces apoptosis in prostate cancer. Cell Physiol Biochem. 2015;37(6):2209–2220. [PubMed: 26610246]
9. Ottman R, Levy J, Grizzle WE, Chakrabarti R. The other face of miR-17–92a cluster, exhibiting tumor suppressor effects in prostate cancer. Oncotarget. 2016;7(45):73739–73753. [PubMed: 27650539]
10. Wang F, Flanagan J, Su N, et al. RNAscope: a novel in situ RNA analysis platform for formalin-fixed, paraffin-embedded tissues. J Mol Diagn. 2012;14(1):22–29. [PubMed: 22166544]
11. Bankhead P, Loughrey MB, Fernandez JA, et al. QuPath: open source software for digital pathology image analysis. Sci Rep. 2017;7(1): 16878. [PubMed: 29203879]
12. Allred DC, Clark GM, Elledge R, et al. Association of p53 protein expression with tumor cell proliferation rate and clinical outcome in node-negative breast cancer. J Natl Cancer Inst. 1993;85(3): 200–206. [PubMed: 8423624]
13. Kim D, Langmead B, Salzberg SL. HISAT: a fast spliced aligner with low memory requirements. Nat Methods. 2015;12(4):357–360. [PubMed: 25751142]
14. SAS Institute Inc. SAS/STAT ® 14.2; 2016

15. Cancer Genome Atlas Research N. The molecular taxonomy of primary prostate cancer. Cell. 2015;163(4):1011–1025. [PubMed: 26544944]
16. Richardsen E, Andersen S, Al-Saad S, et al. Evaluation of the proliferation marker Ki-67 in a large prostatectomy cohort. PLoS One. 2017;12 (11):e0186852. [PubMed: 29141018]
17. Somanathan S, Suchyna TM, Siegel AJ, Berezney R. Targeting of PCNA to sites of DNA replication in the mammalian cell nucleus. J Cell Biochem. 2001;81(1):56–67. [PubMed: 11180397]
18. Rosenthal SA, Hu C, Sartor O, et al. Effect of chemotherapy with docetaxel with androgen suppression and radiotherapy for localized high-risk prostate cancer: the randomized phase III NRG oncology RTOG 0521 trial. J Clin Oncol. 2019;37(14):1159–1168. [PubMed: 30860948]
19. Fei F, Stoddart S, Groffen J, Heisterkamp N. Activity of the Aurora kinase inhibitor VX-680 against Bcr/Abl-positive acute lymphoblastic leukemias. Mol Cancer Ther. 2010;9(5):1318–1327. [PubMed: 20388735]
20. Wu K, Gore C, Yang L, et al. Slug, a unique androgen-regulated transcription factor, coordinates androgen receptor to facilitate castration resistance in prostate cancer. Mol Endocrinol. 2012;26 (9):1496–1507. [PubMed: 22745193]
21. Osorio LA, Farfan NM, Castellon EA, Contreras HR. SNAIL transcription factor increases the motility and invasive capacity of prostate cancer cells. Mol Med Rep. 2016;13(1):778–786. [PubMed: 26648419]
22. Wu K, Zeng J, Zhou J, et al. Slug contributes to cadherin switch and malignant progression in muscle-invasive bladder cancer development. Urol Oncol. 2013;31(8):1751–1760. [PubMed: 22421353]
23. Wu ZQ, Li XY, Hu CY, Ford M, Kleer CG, Weiss SJ. Canonical Wnt signaling regulates Slug activity and links epithelial-mesenchymal transition with epigenetic breast cancer 1, early onset (BRCA1) repression. Proc Natl Acad Sci U S A. 2012;109(41):16654–16659. [PubMed: 23011797]
24. Carpenter RL, Paw I, Dewhirst MW, Lo HW. Akt phosphorylates and activates HSF-1 independent of heat shock, leading to Slug overexpression and epithelial-mesenchymal transition (EMT) of HER2-overexpressing breast cancer cells. Oncogene. 2015;34(5): 546–557. [PubMed: 24469056]
25. Pertea M, Pertea GM, Antonescu CM, Chang TC, Mendell JT, Salzberg SL. StringTie enables improved reconstruction of a transcriptome from RNA-seq reads. Nat Biotechnol. 2015;33(3):290–295. [PubMed: 25690850]
26. Frazee AC, Pertea G, Jaffe AE, Langmead B, Salzberg SL, Leek JT. Ballgown bridges the gap between transcriptome assembly and expression analysis. Nat Biotechnol. 2015;33(3):243–246. [PubMed: 25748911]
27. Wang L, Park HJ, Dasari S, Wang S, Kocher JP, Li WCPAT. Coding-potential assessment tool using an alignment-free logistic regression model. Nucleic Acids Res. 2013;41(6):e74. [PubMed: 23335781]
28. Georgescu C, Corbin JM, Thibivilliers S, et al. A TMEFF2-regulated cell cycle derived gene signature is prognostic of recurrence risk in prostate cancer. BMC Cancer. 2019;19(1):423. [PubMed: 31060542]
29. Chen L, Hong C, Chen EC, et al. Genetic and epigenetic regulation of the organic cation transporter 3, SLC22A3. Pharmacogenomics J. 2013;13(2):110–120. [PubMed: 22231567]
30. Lee Y, Ko D, Min HJ, et al. TMPRSS4 induces invasion and proliferation of prostate cancer cells through induction of Slug and cyclin D1. Oncotarget. 2016;7(31):50315–50332. [PubMed: 27385093]
31. Vias M, Massie CE, East P, et al. Pro-neural transcription factors as cancer markers. BMC Med Genomics. 2008;1:17. [PubMed: 18489756]
32. Kosaka T, Hongo H, Miyazaki Y, Nishimoto K, Miyajima A, Oya M. Reactive oxygen species induction by cabazitaxel through inhibiting Sestrin-3 in castration resistant prostate cancer. Oncotarget. 2017;8 (50):87675–87683. [PubMed: 29152111]
33. Pathak BR, Breed AA, Apte S, Acharya K, Mahale SD. Cysteine-rich secretory protein 3 plays a role in prostate cancer cell invasion and affects expression of PSA and ANXA1. Mol Cell Biochem. 2016;411 (1–2):11–21. [PubMed: 26369530]

34. Grelet S, Andries V, Polette M, et al. The human NANOS3 gene contributes to lung tumour invasion by inducing epithelial-mesenchymal transition. J Pathol. 2015;237(1):25–37. [PubMed: 25904364]
35. Huarte M The emerging role of lncRNAs in cancer. Nat Med. 2015; 21(11):1253–1261. [PubMed: 26540387]
36. Lu W, Tao X, Fan Y, et al. LINC00888 promoted tumorigenicity of melanoma via miR-126/CRK signaling axis. Onco Targets Ther. 2018; 11:4431–4442. [PubMed: 30104884]
37. Wong RS. Apoptosis in cancer: from pathogenesis to treatment. J Exp Clin Cancer Res. 2011;30:87. [PubMed: 21943236]
38. Hanahan D, Weinberg RA. Hallmarks of cancer: the next generation. Cell. 2011;144(5):646–674. [PubMed: 21376230]
39. Campbell K, Casanova J. A common framework for EMT and collective cell migration. Development. 2016;143(23):4291–4300. [PubMed: 27899506]
40. Medici D, Hay ED, Olsen BR. Snail and Slug promote epithelial-mesenchymal transition through beta-catenin-T-cell factor-4-dependent expression of transforming growth factor-beta3. Mol Biol Cell. 2008;19(11):4875–4887. [PubMed: 18799618]
41. Uygur B, Wu WS. SLUG promotes prostate cancer cell migration and invasion via CXCR4/CXCL12 axis. Mol Cancer. 2011;10:139. [PubMed: 22074556]
42. Singh S, Sadacharan S, Su S, Belldegrun A, Persad S, Singh G. Overexpression of vimentin: role in the invasive phenotype in an androgen-independent model of prostate cancer. Cancer Res. 2003;63(9):2306–2311. [PubMed: 12727854]
43. Putzke AP, Ventura AP, Bailey AM, et al. Metastatic progression of prostate cancer and e-cadherin regulation by zeb1 and SRC family kinases. Am J Pathol. 2011;179(1):400–410. [PubMed: 21703419]
44. Murillo-Garzon V, Kypta R. WNT signalling in prostate cancer. Nat Rev Urol. 2017;14(11):683–696. [PubMed: 28895566]
45. Chen C, Cai Q, He W, et al. AP4 modulated by the PI3K/AKT pathway promotes prostate cancer proliferation and metastasis of prostate cancer via upregulating L-plastin. Cell Death Dis. 2017;8(10):e3060. [PubMed: 28981098]
46. de Aberasturi AL, Calvo A. TMPRSS4: an emerging potential therapeutic target in cancer. Br J Cancer. 2015;112(1):4–8. [PubMed: 25203520]
47. Kim S, Ko D, Lee Y, et al. Anti-cancer activity of the novel 2-hydroxydiarylamide derivatives IMD-0354 and KRT1853 through suppression of cancer cell invasion, proliferation, and survival mediated by TMPRSS4. Sci Rep. 2019;9(1):10003. [PubMed: 31292507]
48. Kozak J, Wdowiak P, Maciejewski R, Torres A. Interactions between microRNA-200 family and Sestrin proteins in endometrial cancer cell lines and their significance to anoikis. Mol Cell Biochem. 2019;459(1–2):21–34. [PubMed: 31073887]
49. Shan J, Al-Muftah MA, Al-Kowari MK, et al. Targeting Wnt/-EZH2/microRNA-708 signaling pathway inhibits neuroendocrine differentiation in prostate cancer. Cell Death Discov. 2019;5:139. [PubMed: 31583122]
50. Chen X, Corbin JM, Tipton GJ, Yang LV, Asch AS, Ruiz-Echevarria MJ. The TMEFF2 tumor suppressor modulates integrin expression, RhoA activation and migration of prostate cancer cells. Biochim Biophys Acta. 2014;1843(6):1216–1224. [PubMed: 24632071]
51. Kailiang L, Wenjing G, Jie X, Aikun W, Hongchao H. Expression of TMEFF2 in human pancreatic cancer tissue and the effects of TMEFF2 knockdown on cell, proliferation, and apoptosis in human pancreatic cell lines. Medical Science Monitor. 2019;25:3238–3246. 10.12659/msm.913974. [PubMed: 31044775]
52. Fu L, Qin YR, Ming XY, et al. RNA editing of SLC22A3 drives early tumor invasion and metastasis in familial esophageal cancer. Proc Natl Acad Sci U S A. 2017;114(23):E4631–E4640. [PubMed: 28533408]

What's new?

Long non-coding RNAs have emerged as key regulatory molecules that are frequently aberrantly expressed in cancers. Here, the authors show that *PAINT* plays an oncogenic role in prostate cancer progression through modulation of the apoptosis, drug resistance, and epithelial-mesenchymal transition gene networks. Furthermore, analysis of expression levels in patient tissues and transcriptome profiling of *PAINT*-expressing cells offer a global perspective on the involvement of *PAINT* in prostate cancer progression. The findings highlight the potential of *PAINT* to serve as a therapeutic target in treatment of aggressive prostate cancer.

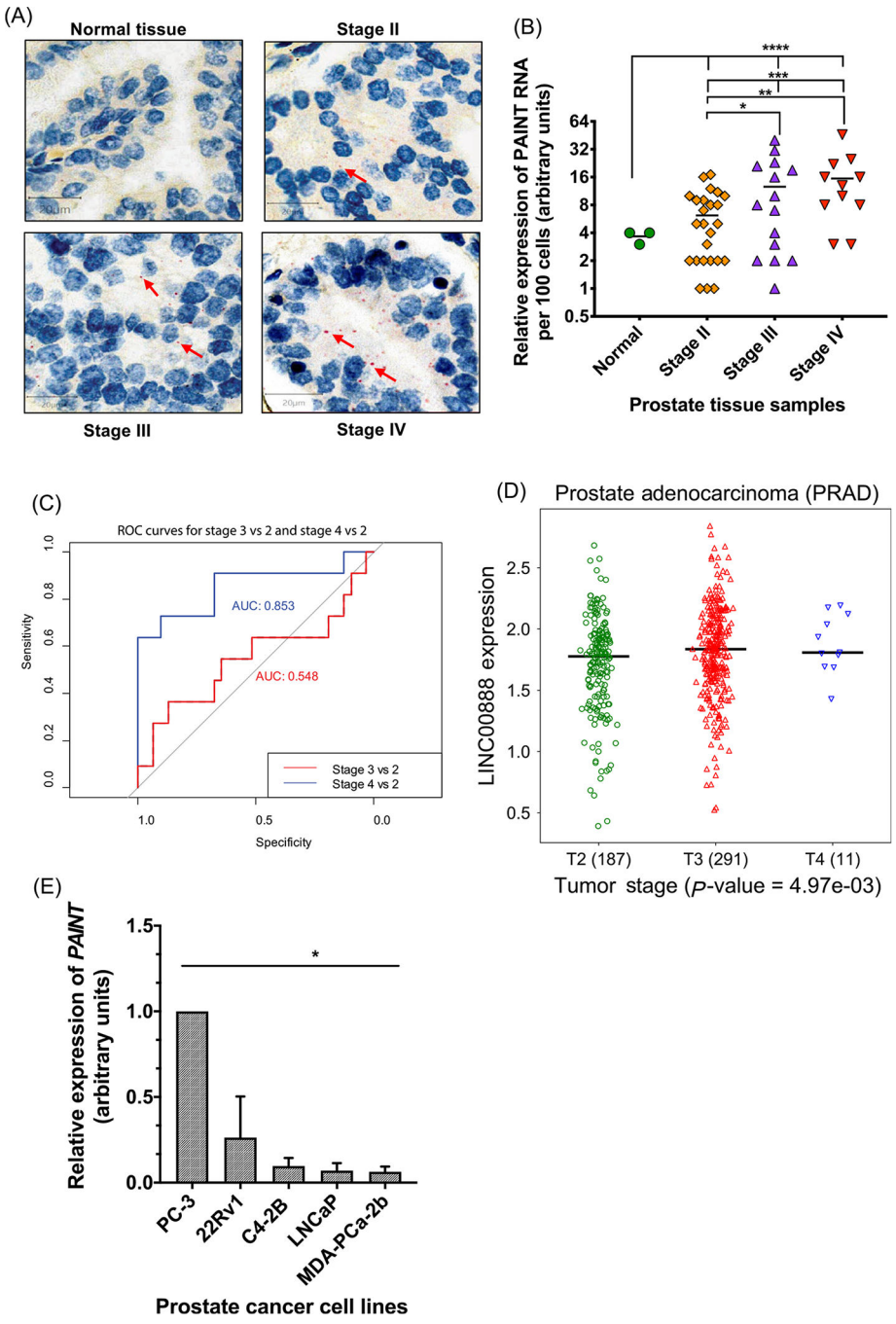

FIGURE 1.

PAINT is upregulated in late stage prostate cancer. A, Representative TMA images of *PAINT* RNA-ISH in tissues from normal prostate stage II, stage III and stage IV PCa. Arrows: positive signals (Red dots). B, Comparative expression analysis of *PAINT* in prostate cancer and normal tissues **P*-value = .02, ***P*-value = .0022, ****P*-value = .013, *****P*-value = .016. C, Receiver operating characteristic (ROC) curves based on the two models. Blue line illustrates that the area under the ROC curve is 0.86 confirming a high level of accuracy of predicting stage IV vs stage I/II. Red line illustrates a poor level of

accuracy of predicting stage III vs stage I/II. D, Analysis of RNA-seq data using TCGA PRAD dataset shows higher expression of *PAINT* (LINC00888) in stage III and stage IV compared to stage II PCa tissues. E, Expression analysis showing highest expression of *PAINT* in metastatic PC-3 cells. Data represent mean ± SD of three biological replicates. * $P < .0001$

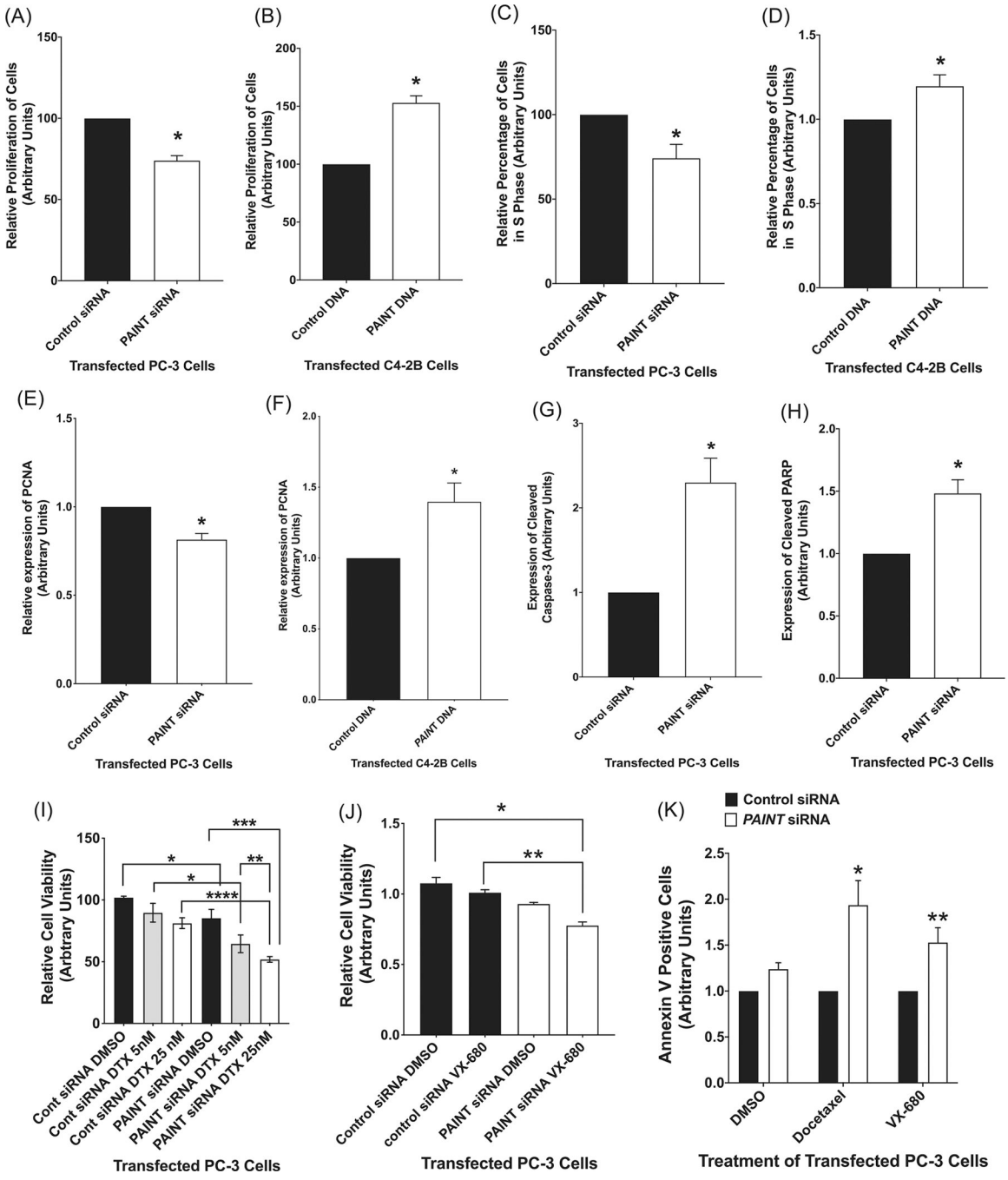

FIGURE 2.

Changes in *PAINT* expression regulate cell proliferation, cell cycle progression, cell survival and drug sensitivity. A, MTS assays showing proliferation of PC-3-*PAINT*^{si} and PC-3^{C} cells. Data show the mean ± SD of three biological replicates. **P*-value = .004. B, MTS assays showing proliferation of C4-2B-*PAINT*$^{++}$ and C4-2B^{C} cells. Data represent the mean ± SD of three biological replicates. **P*-value = .004. C, Comparative analysis of S phase cells exhibited a reduction in the S phase population of PC-3-*PAINT*^{si} cells compared to PC-3^{C} cells. Data show the mean ± SD of four biological replicates. **P*-value

= .008. D, Comparative analysis of S phase cells showing an increase (19%) in S phase population of C4-2B-*PAINT*$^{++}$ cells compared to C4-2B^{C} subline. Data represent the mean ± SD for three biological replicates. **P*-value = .036. E and F, Densitometric analysis of PCNA in PC-3-*PAINT*^{si} and C34–2B-*PAINT*s^{++} with **P*-value = .029 and **P*-value = .024, respectively. G and H, Densitometric analysis of cleaved Caspase −3 and activated PARP in PC-3-*PAINT*^{si} cells compared to PC-3^{C} cells with **P*-value = .045 and ***P*-value = .016, respectively. Data show the mean ± SD of three individual experiments. I, Viability assays of PC-3-*PAINT*^{si} and PC-3^{C} cells in combination with DTX or DMSO treatments. Data show the mean ± SD of three individual experiments. **P*-value = .015, ***P*-value = .022, ****P*-value = .001, *****P*-value = .0005. J, Viability assay of PC-3-*PAINT*^{si} cells to VX-680 treatments compared to DMSO and PC-3^{C} cells. Data show the mean ± SD of three individual experiments. **P*-value = .0037, ***P*-value = .0002. K, Enumeration of Annexin V positive cells upon DTX (5 nM) and VX-680 (25 nM) treatment of PC-3-*PAINT*^{si} cells compared to PC-3^{C} cells

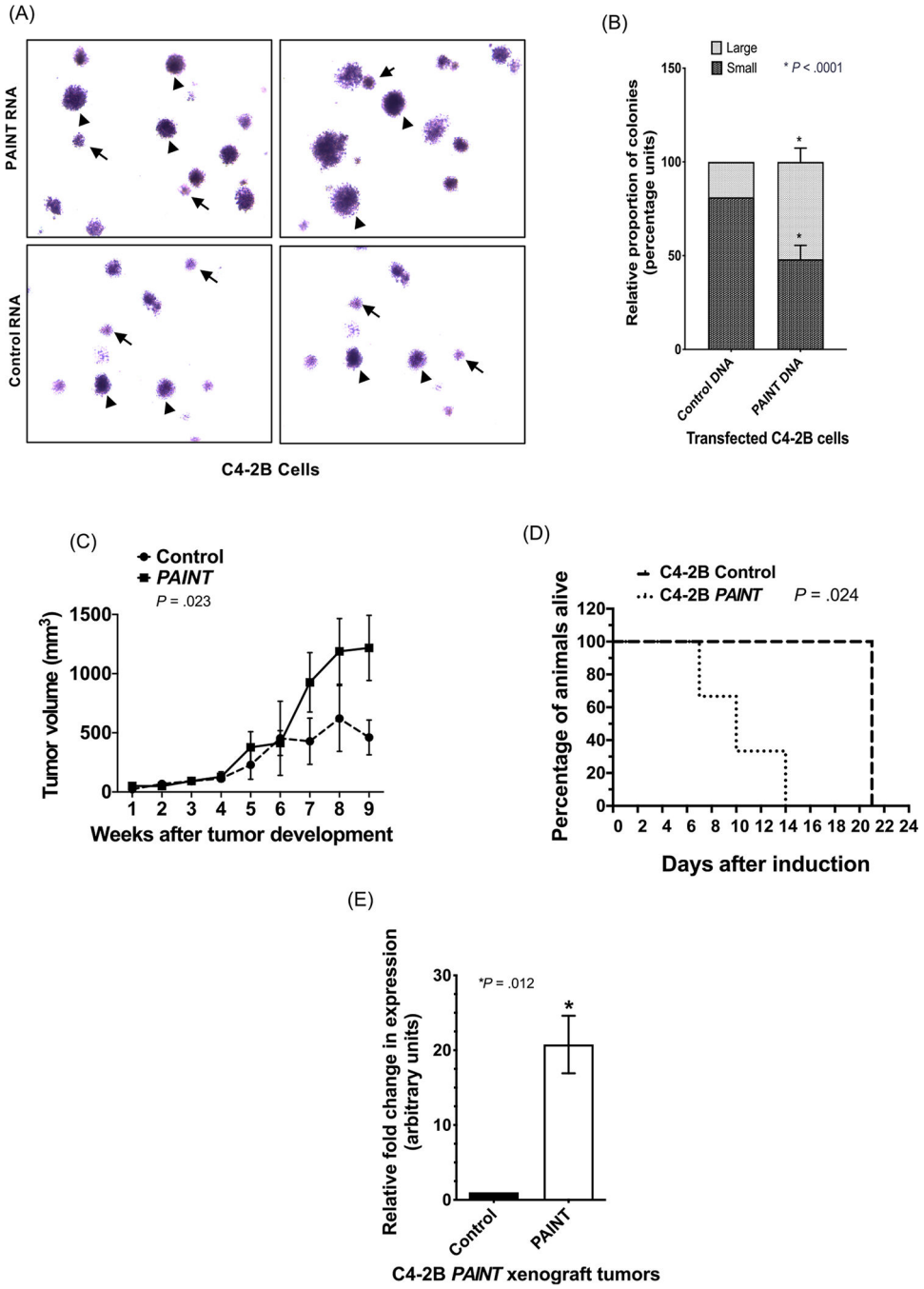

FIGURE 3.

PAINT promotes colony formation and tumor growth in xenograft models. A, Representative images of soft agar colonies formed by C4-2B-*PAINT*$^{++}$(top panels) and C4-2B^{C} cells (bottom panels). Arrowheads represent large colonies and small arrows represent small colonies. B, Quantitative analysis of the small (<7 μm) and large (>7 μm) of colonies formed by C4-2B-*PAINT*$^{++}$ cells compared to C4-2B^{C} cells. Data show the mean ± SD of three biological replicates. **P*-value < .0001. C, Progression of tumor growth following injection of C4-2B-*PAINT*$^{++}$ and C4-2B^{C} cells in the flank of NSG

mice. Tumor growth was monitored by tumor volume measurement for 9 weeks post development of visible tumors. Data show the mean ± SD of 3 mice/group. *P*-value = .0008. D, Inducible C4-2B-*PAINT*^{I} xenografts with Dox-induced expression of *PAINT* were alive for significantly shorter time based on the time elapsed to reach the specified 1.5 cm^3 volume and compared to the uninduced control group (C4-2B-Control). Data show the mean ± SD of 3 mice/group. *P*-value = 0.024. E, qRT-PCR showing increased expression of *PAINT* in tumors from mice injected with C4-2B-*PAINT*$^{++}$ cells compared to mice injected with C4-2B^{C} cells. Data show the mean ± SD of 3 mice/group. **P*-value = .01

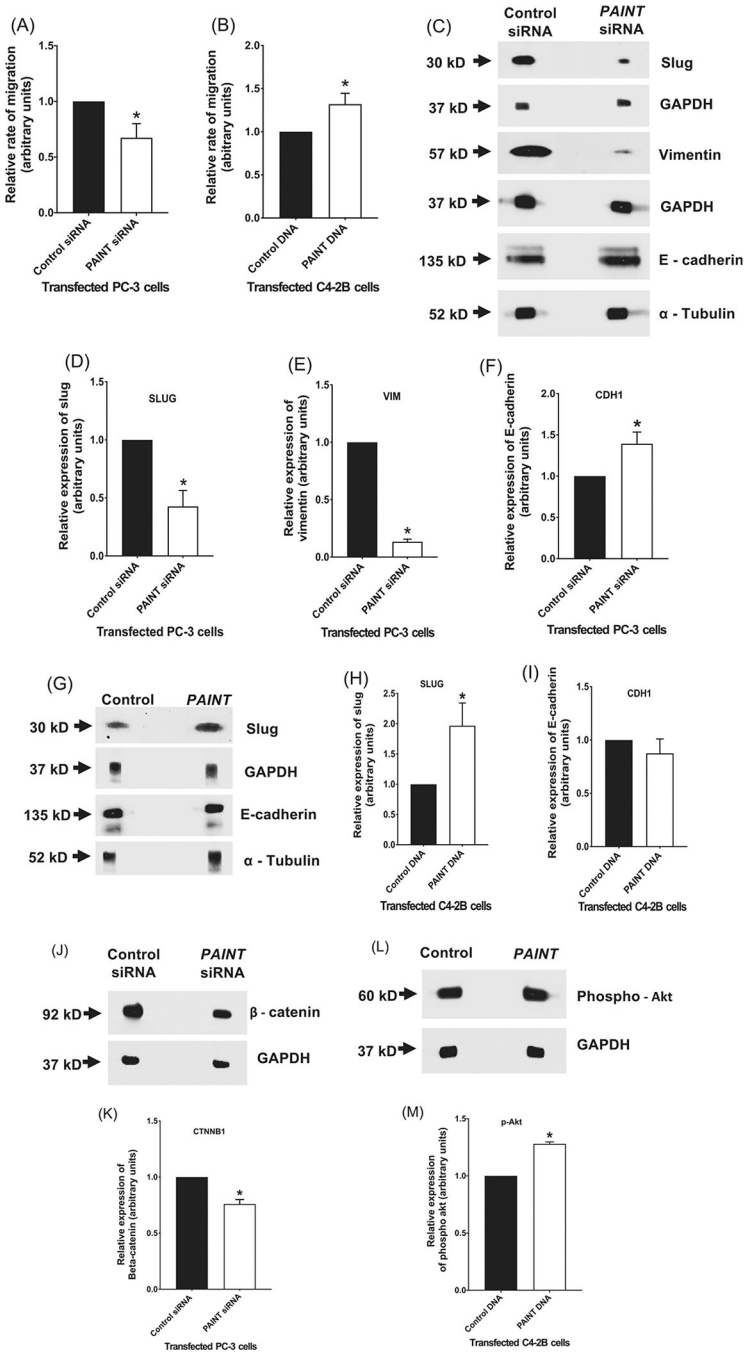

FIGURE 4.

PAINT promotes migration and epithelial-mesenchymal transition through modulation of multiple proteins. A, Analysis of the rate of migration of PC-3-*PAINT*^{si} cells compared to PC-3^{C} cells. Data show the mean ± SD of three independent experiments. **P* = .046. B, Analysis of the rate of migration of C4-2B-*PAINT*$^{++}$ cells compared to C4-2B^{C} cells. Data represent mean ± SD for three biological replicates. **P*-value = .01. C, Western blots showing altered expression of Slug, Vimentin and E-cadherin in PC-3-*PAINT*^{si} and PC-3^{C} cell lysates. GAPDH and α-tubulin were used as the loading controls. D-F, Densitometry of

Slug, Vimentin and E-cadherin expression in PC-3-*PAINT*^{si} and PC-3^{C} cells. Data show the mean ± SD of three biological replicates. **P*-value = .018, ***P*-value = .0002, ****P*-value = .011. G, Western blots showing expression of Slug and E-cadherin in C4-2B-*PAINT*$^{++}$ and C4-2B^{C} cell lysates. GAPDH and α-tubulin were used as the loading controls. H and I, Densitometry of Slug and E-cadherin expression in C4-2B-*PAINT*$^{++}$ or C4-2B^{C} cells. Data show the mean ± SD of three biological replicates. **P*-value = .047. J, Western blots of B-Catenin upon knockdown of *PAINT* in PC-3 cells, and GAPDH as the loading control. K, Densitometric analysis of B-Catenin expression upon *PAINT* inhibition. Data represent mean ± SD. **P*-value = .009. L, Western blots of phospho-Akt upon overexpression of *PAINT* in C4-2B cells and GAPDH as the loading control. M, Densitometric analysis of phospho-Akt expression in C4-2B-*PAINT*$^{++}$ subline compared to C4-2B^{C} cells. Data represent mean ± SD. **P*-value = .0013

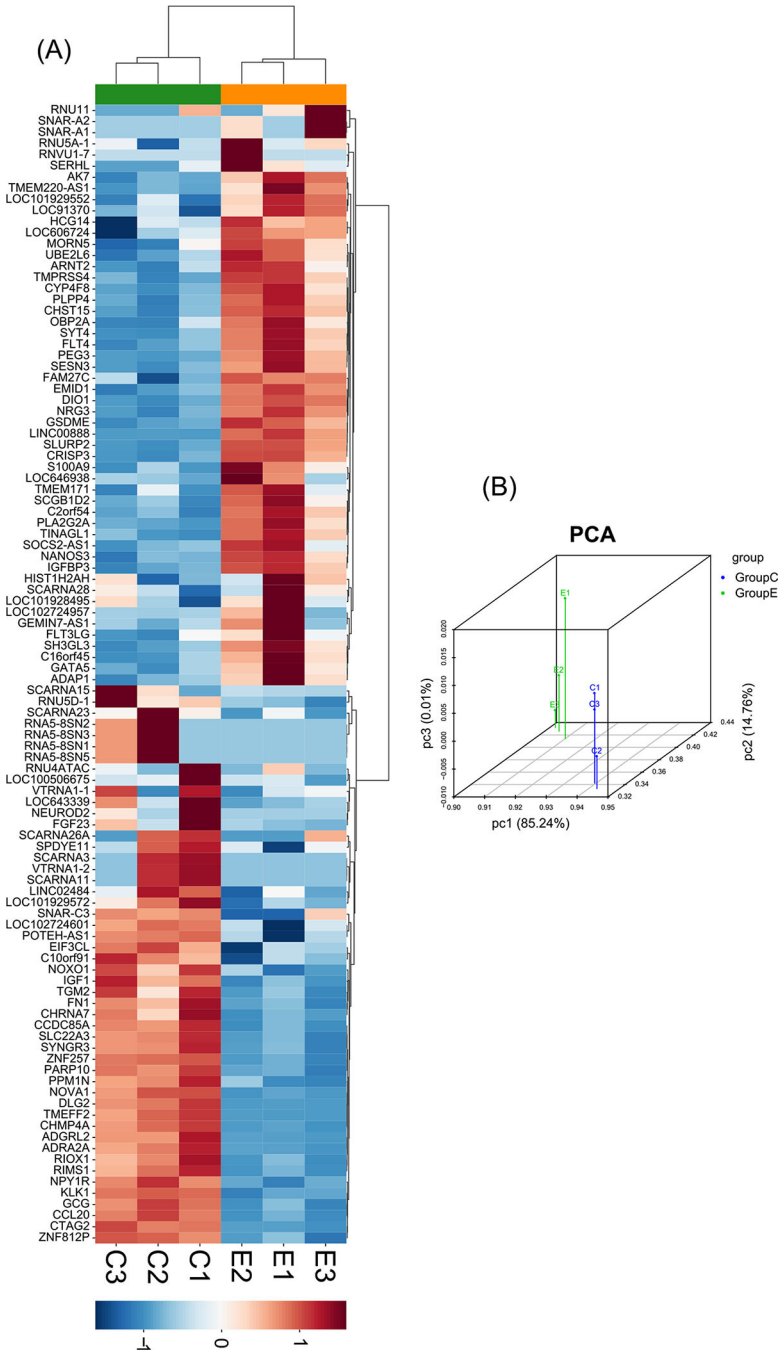

FIGURE 5.

Transcriptome analysis reveals significantly dysregulated genes in *PAINT* overexpressing C4-2B cells. A, Hierarchical Clustering analysis showed a significant number of differentially expressed genes between C4-2B-*PAINT*$^{++}$ (E group) and C4-2B^{C} cells (C group). Genes are represented by rows and samples are represented by columns. Red color indicates higher expression and green color indicates lower expression. B, PCA of three biological replicates of C4-2B-*PAINT*$^{++}$ cells compared to C4-2B^{C} cells exhibited distinguishable gene expression profiles between the two groups

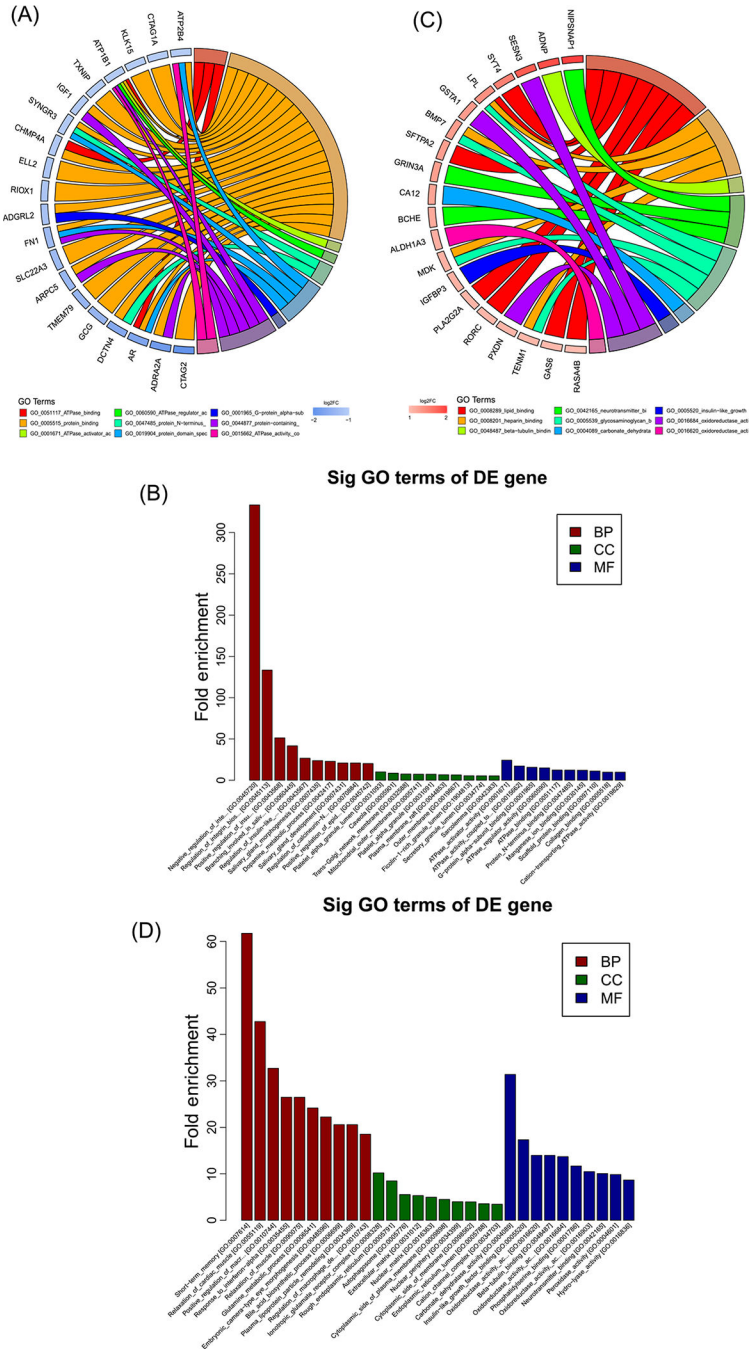

FIGURE 6.

GO enrichment analysis of differentially expressed genes between *PAINT* expressing C4-2B cells and control cells. A and C, Circular plots of GO enrichment analysis showing 20 downregulated genes and 20 upregulated genes in C4-2B-*PAINT*$^{++}$ cells and their molecular functions, respectively. B and D, Top 10 enriched GO terms for significantly downregulated genes and upregulated genes in C4-2B-*PAINT*$^{++}$ cells based on biological process (BP), cellular component (CC) and molecular function (MF), respectively. The order of the bars is based on *P*-value from left to right (−log 10)

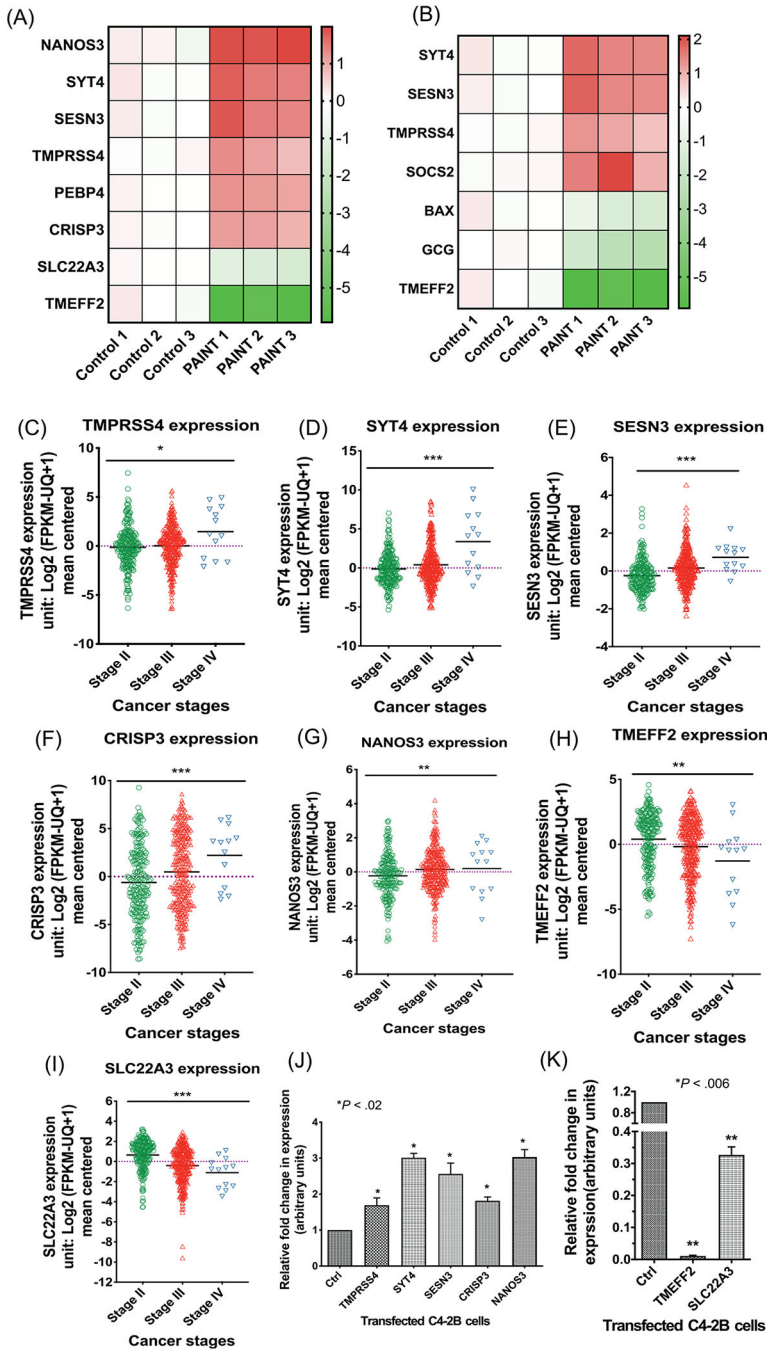

FIGURE 7.

Functional analysis and validation of dysregulated genes in *PAINT* overexpressing prostate cancer cells. A and B, Expression heat map showing differential expression (Log_2-fold) of genes involved in apoptosis (A) and EMT-regulated genes (B) between individual samples of C4-2B-*PAINT*$^{++}$ (right) and C4-2B^{C} cells (left). Three biological replicates were included for each group. **P*-value < .05. C-I, Expression of apoptosis and EMT related genes showing significant differences between stage II (n = 218) and stage III (313) and IV (n = 13) based on TCGA PRAD gene set analysis: TMPRSS4 (*P* = .02697) (C), SYT4 (*P*

= .0041) (D), SESN3 (*P*-value < .0001) (E), CRISP3 (*P*-value = .0006) (F), NANOS3 (*P*-value = .0037) (G) TMEFF2 (*P*-value = .0018) (H) and SLC22A3 (*P*-value < .0001) (I). J, qRT-PCR validation of the selected five upregulated genes, TMPRSS4, SYT4, SESN3, CRISP3 and NANOS3 in C4-2B-*PAINT*$^{++}$ and C4-2B^{C} cells. Data show the mean ± SD of three biological replicates. **P*-value < .05. K, qRT-PCR validation of the selected two downregulated genes, TMEFF2 and SLC22A3 in C4-2B-*PAINT*$^{++}$ and C4-2B^{C} cells. Data show the mean ± SD of three biological replicates. **P*-value <.05